A DC-Coupled High Dynamic Range Biomedical Radar Sensor With Fast-Settling Analog DC Offset Cancelation

Dongyang Tang, *Student Member, IEEE*, Jing Wang, *Student Member, IEEE*, Weibo Hu, *Member, IEEE*, Zhengyu Peng, *Student Member, IEEE*, Yi-Chyun Chiang, *Senior Member, IEEE*, and Changzhi Li, *Senior Member, IEEE*

***Abstract*— One challenge of designing a dc-coupled biomedical radar sensor is dealing with the dc offset voltage presented in its receiver. The undesired dc offset is mainly caused by clutter reflection and hardware imperfection. It may saturate the baseband amplifier and limit the maximum dynamic range that a biomedical radar sensor can achieve. AC-coupling the signal can eliminate dc offset but it will also distort the signal, and thus may not be acceptable for high precision applications. In this paper, a dc-coupled biomedical radar sensor is proposed incorporating an analog dc offset cancelation circuit with fast start-up feature. It can automatically remove any dc offset in the baseband signal and emulates an ac-coupling system. It can also be easily reconfigured into a dc-tracking mode when application requires. When entering this mode, the initial dc offset will be removed, whereas future dc change can be recorded. The proposed solution only uses analog components without requiring any digital signal processing nor software programing. Therefore, compared with the existing digitized dc offset calibration techniques, the proposed method has the advantage of low cost, easy implementation, short delay, and high resolution. The experiment results demonstrated that a wide range of dc offset can be successfully removed from the biomedical radar sensor, and its dynamic range can be maximized. The reconfiguration of the dc-tracking mode has also been tested and verified. Furthermore, the proposed dc offset cancelation circuit has the potential to be easily adopted by other systems that also face the dc offset problem.**

***Index Terms*— Biomedical radar sensor, DC offset cancelation, Doppler radar, dynamic range, homodyne receiver, noncontact sensor, vital signs detection.**

Manuscript received July 24, 2018; revised November 9, 2018; accepted December 8, 2018. Date of publication January 8, 2019; date of current version April 17, 2019. This work was supported by the National Science Foundation under Grant ECCS-1254838, Grant CNS-1718483, and Grant ECCS-1808613. The Associate Editor coordinating the review process was Yuri Alvarez Lopez. *(Corresponding author: Changzhi Li.)*

D. Tang, J. Wang, and C. Li are with the Department of Electrical and Computer Engineering, Texas Tech University, Lubbock, TX 79409 USA (e-mail: dongyang.tang@ttu.edu; anna.wang@ttu.edu; changzhi.li@ttu.edu).

W. Hu is with the College of Electronic Information and Optical Engineering, Nankai University, Tianjin 300071, China (e-mail: weibohu@hotmail.com).

Z. Peng is with Aptiv Corporation, Kokomo, IN 46902 USA (e-mail: zpeng.me@gmail.com).

Y.-C. Chiang is with the Department of Electronic Engineering, Chang Gung University, Taoyuan, Taiwan (e-mail: ycchiang@mail.cgu.edu.tw).

Color versions of one or more of the figures in this paper are available online at http://ieeexplore.ieee.org.

Digital Object Identifier 10.1109/TIM.2018.2888917

I. Introduction

RADAR systems are widely used as noncontact sensors in a variety of measurement systems. One of the applications is noncontact monitoring of respiration and heartbeat. Pioneering works using radar sensor for vital signs detection can be traced back to the last century [1]–[3]. In recent years, together with the blooming industry of Internet of Things and portable healthcare devices, noncontact biomedical radar sensors have gained great momentum in both research and industrial world [4]–[19]. Thanks to the Moore's law, the entire radar sensor can now be integrated into a single system-on-chip solution [19]–[23]. This permits radar sensors to be realized with very low cost, low power, and portable size.

Different types of radar systems have been studied as biomedical sensors. The most popular one is Doppler radar [4], [5], [17]–[21], [24], [25]. Recently, vital signs detection using frequency-modulated continuous-wave (FMCW) radar, ultra-wideband radar, and frequency shift-keying (FSK) radar have also been published [5]–[10]. The majority of the receivers of the biomedical radar sensors adopt the homodyne architecture for the advantage of low power and low cost compared with the heterodyne architecture. However, one disadvantage of the homodyne architecture is the dc offset presented at the output of the receiver mixer [18], [19], [21], [25]–[30]. The dc offset due to hardware imperfection have random part-to-part variations and temperature variations, whereas the dc offset caused by clutter reflections vary a lot with the experiment setup and surrounding environment. Both dc offset sources are unpredictable, while the clutter reflection maybe dominant. The resulting dc offset may saturate the baseband amplifier and limit the system dynamic range.

One way to solve this issue is ac coupling the output of the mixer to the baseband amplifier [5]. However, it inevitably distorts the input signal as the dc information is blocked and some low-frequency components are attenuated. This can be unacceptable in certain high precision applications such as unique identification [18] and medical diagnosis [30]. Several different techniques to address the dc offset in a dc-coupled biomedical radar system have been proposed in the literature. Initially, people used manual calibration to tune out the dc offset [25]. It requires manual calibration with external equipment to measure the dc offset and the tuning process

needs to be applied every time the dc offset changes. In [30], an adaptive feedback loop was proposed to adjust the dc bias of the operational amplifier (op-amp) and keep the amplifier out of saturation. The amplifier output is sampled by an analog-to-digital converter (ADC) first. Then a software algorithm is used to monitor the ADC output and will change the bias of the amplifier to a different setting when saturation happens. However, it may take a few iterations before the circuit recover from saturation. This process can be done automatically but it requires external equipment and software programing. In [19], a customized integrated circuit (IC) with an op-amp and a current based digital-to-analog converter (DAC) was designed to tune the dc offset. It eliminates the need for external equipment, yet still requires the help from software. A couple of different implementations of canceling the dc offset using adaptive feedback loop are also published in [21] and [29]. One disadvantage of involving software as part of the feedback loop is that it takes a long time for the circuit to settle and for the calibration algorithm to converge due to the iterative interaction between software and hardware. The settling time is on the order of seconds. In addition, the feedback loop solution is potentially vulnerable to the loop stability issue, and the delay in the feedback path affects the stability. Another problem is that they must have interfaces between analog and digital world, i.e., both ADC and DAC are needed. The quantization noise from ADC and the mismatch from DAC will limit the resolution of the calibration algorithm.

Previously, an analog dc offset calibration solution was proposed for differential input signals in [28], which does not require external equipment nor software. In this paper, a dc-coupled biomedical radar sensor is proposed with fast-settling analog dc offset cancelation circuit designed for its single-ended receiver output. The proposed technique adopts analog feedforward technique to remove the dc offset presented in the receiver, which inherently does not have stability concern. It can operate in two different modes for different applications. One mode removes the dc offset continuously and emulates an ac-coupling system. This mode works for applications that can tolerate dc and low-frequency distortion. The advantage for this mode is that it is immune to dc offset drift caused by environment change since it keeps monitoring and removing any dc change in the system. The other mode records dc input changes after removing the initial dc offset in the system at powering up. It provides high precision recording for the input signal but suffers from dc offset drift problem. It is suitable for applications where the environment does not change significantly and thus presenting a small dc offset drift. The settling time or start-up time of the proposed solution is much shorter than adaptive feedback solutions and can be considered negligible for most of the applications. Since the entire system is built with analog components, the ADC quantization noise and the DAC mismatch effect are eliminated. The resolution of the designed architecture is mainly limited by the mismatch of the resistors and the offset of the op-amps, which can be well controlled by mature fabrication and circuit techniques such as chopping and autozeroing [31]. Hence, the resolution is inherently higher than that of the aforementioned digital solutions.

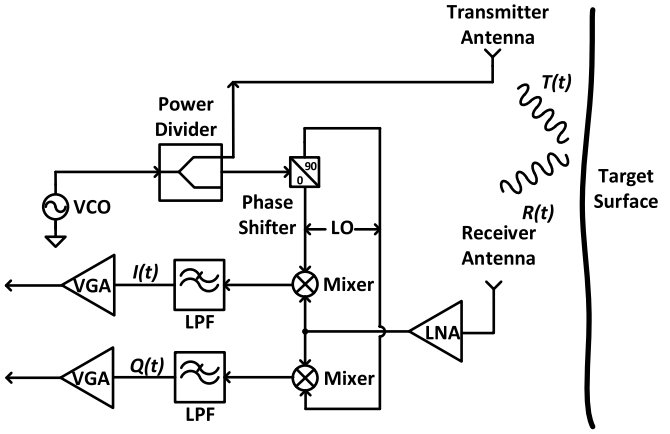

Fig. 1. System block diagram of a conventional dc-coupled homodyne Doppler radar sensor.

In Section II, a review of the hardware design and vital signs sensing theory of a typical biomedical radar sensor with homodyne receiver will be given. Section III introduces the proposed biomedical radar sensor and analog dc cancelation circuit design. The experimental results demonstrating the effectiveness of the proposed dc offset cancelation circuit are presented in Section IV. Finally, conclusions are drawn and suggestions for future works are made in Section V.

II. Review of Doppler Biomedical Radar Sensor

The block diagram of a conventional dc-coupled Doppler radar sensor with the homodyne architecture is shown in Fig. 1. In vital signs sensing scenarios, first, a pure radio frequency (RF) sinusoidal at f Hz is generated by an oscillator. The oscillator is usually implemented as a voltage-controlled oscillator (VCO) so that the frequency is tunable with a control voltage. Then, through a power splitter, half of the RF signal goes to the transmitter antenna and radiates out to the air. The transmit signal $T(t)$ can be expressed as

$$T(t) = \cos(2\pi f t + \Phi(t)) \tag{1}$$

where $\Phi(t)$ is the phase noise of $T(t)$. When the transmitted signal reaches the chest wall of a target, it will be reflected back with its phase modulated by the time-varying body movements $x(t)$ (i.e., respiration and heartbeat). According to [22], the received signal $R(t)$ can be written as

$$R(t) = \cos\left(2\pi f t - \frac{4\pi x(t)}{\lambda} - \frac{4\pi d_0}{\lambda} + \Phi\left(t - \frac{2(x(t)+d_0)}{c}\right)\right) \tag{2}$$

where d_0 represents the nominal distance between the target and radar, λ stands for the wavelength of the RF signal, and c is the speed of light.

After the reflected signal is received by the receiver antenna, it is amplified by a low noise amplifier (LNA) and sent to a mixer for downconversion. A biomedical radar sensor usually has two orthogonal baseband signals $I(t)$ and $Q(t)$ to eliminate the null detection point problem [20], [25]. $I(t)$ and $Q(t)$ are generated by mixing the received signal

with the in-phase and quadrature local oscillator (LO) signals. In a homodyne receiver, the LO frequency is the same as the transmitted frequency, so that only one VCO is needed. This is one of the reasons that homodyne receivers usually have lower cost and lower power consumption. In a typical quadrature homodyne receiver, the in-phase LO signal is the same as the transmitted signal $T(t)$, while the quadrature one has 90° phase shift from $T(t)$. After downconversion, a low-pass filter (LPF) is used to filter out undesired high-frequency components in the baseband outputs. The baseband signals can be represented as

$$I(t) = A_I \cos\left(\frac{4\pi x(t)}{\lambda} + \Phi(t) - \Phi\left(t - \frac{2(x(t)+d_0)}{c}\right) + \frac{4\pi d_0}{\lambda}\right) \tag{3}$$

$$Q(t) = A_Q \sin\left(\frac{4\pi x(t)}{\lambda} + \Phi(t) - \Phi\left(t - \frac{2(x(t)+d_0)}{c}\right) + \frac{4\pi d_0}{\lambda}\right) \tag{4}$$

where A_I and A_Q are gains for I and Q channels, respectively. The phase noise terms $\Phi(t)$ and $\Phi(t-((2(x(t)+d_0))/c))$ are correlated since they are originated from the same source but with a different delay. The difference between these two terms is very small and negligible in short-range applications according to the range correlation theory [20], [32]. An intuitive way to understand this is that the delay is very small for short range applications so that low-frequency noise cannot change much during that time. Thus, (3) and (4) can be simplified as

$$I(t) = A_I \cos\left(\frac{4\pi x(t)}{\lambda} + \frac{4\pi d_0}{\lambda}\right) \tag{5}$$

$$Q(t) = A_Q \sin\left(\frac{4\pi x(t)}{\lambda} + \frac{4\pi d_0}{\lambda}\right). \tag{6}$$

Finally, $I(t)$ and $Q(t)$ are sent for amplification before postprocessing. Usually, a data acquisition device records $I(t)$ and $Q(t)$. Algorithms such as the complex demodulation or the arctangent demodulation will be applied in the digital domain to recover the respiration and heartbeat [25], [33], [34].

To achieve the best dynamic range for the system, the baseband amplifier needs to provide as much gain as possible without saturation. For different input signal levels, the amount of gain needed is different. Therefore, a variable gain amplifier (VGA) is more suitable instead of a fixed gain amplifier. However, if the VGA sees a large dc offset at its input on top of the signals of interest, the dc offset will also be amplified and may saturate the amplifier. In this case, the gain of the VGA must be reduced to avoid saturation and the dynamic range is sacrificed.

As mentioned before, there are mainly two sources that cause dc offset at the input of the VGA: hardware imperfection and stationary clutter reflection. Any mismatch from nonideal hardware components will results in a dc offset. Besides, LO leakage is another common hardware dc offset contributor [35]. The dc offset originated from clutter reflection is caused by the reflections from stationary objects near the target. If an object is stationary and in the sight of the radar, the signal reflected back will have the same frequency as the transmitted signal but with a constant phase shift related to the range to the object. After downconversion, the constant phase shift becomes a dc voltage at the output of mixer. This is a special case for (5) and (6). Assuming $x(t)$ is constant, $I(t)$ and $Q(t)$ reduce to constant dc values. Depending on the location, geometry, and material of the stationary object, the dc offset changes accordingly.

III. Proposed Biomedical Radar Sensor With Analog DC Offset Cancelation Circuit

The first part of this section covers the system design of the proposed biomedical radar sensor and the second part focus on the fast-settling analog dc offset cancelation circuit.

A. System Design of the Proposed Biomedical Radar Sensor

Fig. 2 shows the system architecture of the proposed biomedical radar sensor. It includes a mode control module, an RF transceiver, and baseband circuits. Although the primary focus of this paper is Doppler radar, the proposed biomedical radar can operate in three different modes: Doppler mode, FMCW mode, and FSK mode. Mode selection is achieved by applying different control signals to the VCO. The Doppler mode uses a fixed dc bias for the VCO to generate a single-frequency signal. When the FMCW mode is chosen, a sawtooth waveform is used to continuously modulate the output frequency of the VCO and a reference pulse sequence (RPS) is used to synchronize with the period of the frequency modulation. A simple analog circuit is used to generate the sawtooth waveform and RPS, which is detailed in [5]. It consists of a two-input integrator, a hysteresis comparator, and two diodes. In the FSK mode, the control signal of the VCO is a square wave. It is generated with an op-amp together with the existing FMCW control waveform generation circuit. Two different voltage levels of the square wave define the two output frequencies of the VCO.

The radar transceiver design is similar to the basic architecture shown in Fig. 1. On the transmitter path, a power amplifier (PA) is inserted before the transmitter antenna to deliver a maximum transmit power of 18 dBm to the transmitter antenna. A passive I/Q mixer (HMC 525) is chosen in this design to minimize the flicker noise [23], since vital signs signals normally have very low frequencies. A gain stage is added to increase the LO input voltage swing of the mixer. One disadvantage of this passive mixer is that its outputs swing to negative voltage. Therefore, to save the cost of generating a negative supply on board, a level shifter is added to shift up the output of the mixer to achieve a positive voltage swing. The level shifter is built as an inverting amplifier with an op-amp. The inversion of signal caused by this inverting amplifier does not affect the result, since both the I and Q channels are matched and inverted at the same time. Ideally, the gain of this inverting amplifier should be large enough so that the output swing is maximized. However, due to the dc offset at the output of the mixer, the gain of this amplifier is set low to avoid the worst-case dc offset from saturating the detector. Therefore, it is important to have a VGA that can deal with different input dc offsets voltage

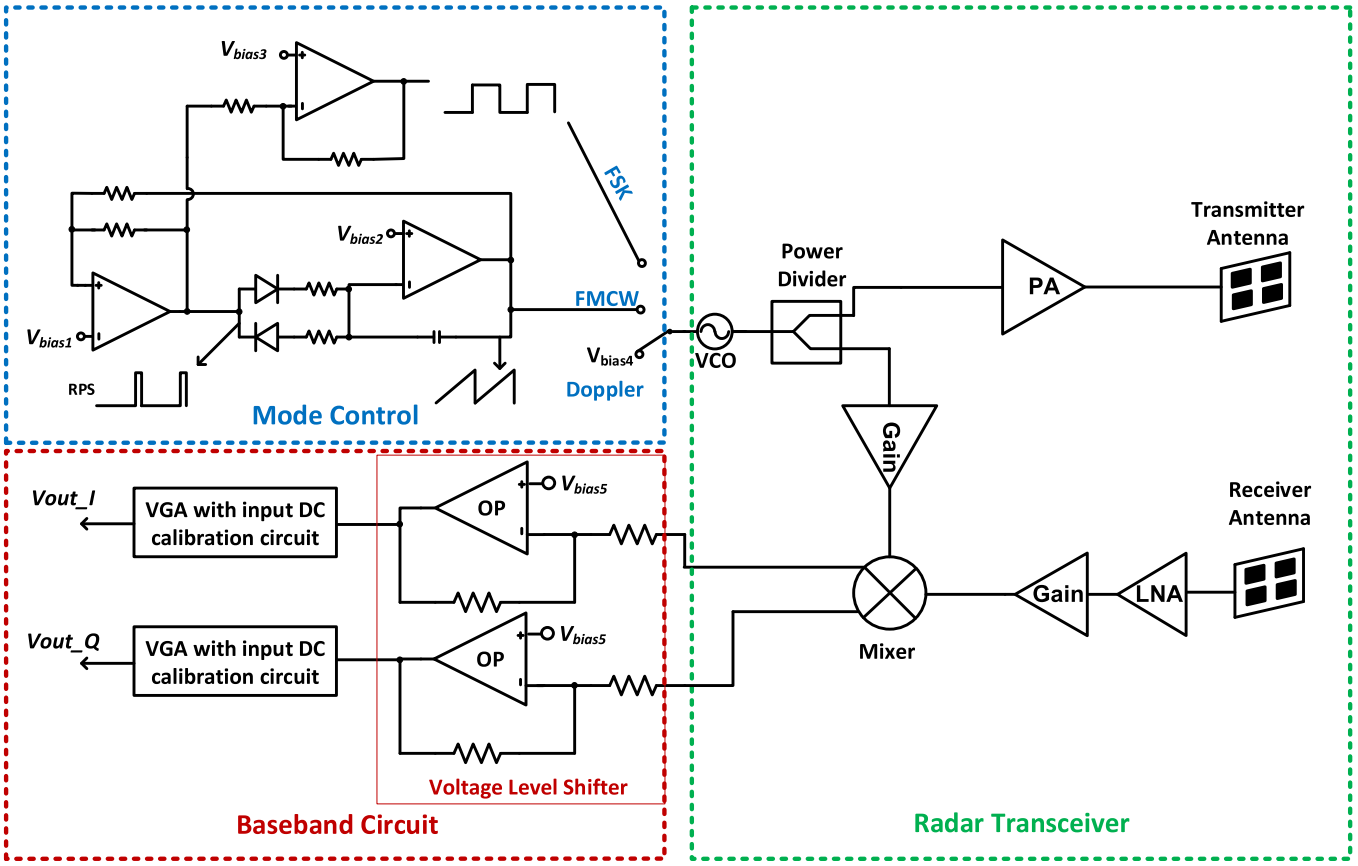

Fig. 2. Proposed biomedical radar sensor system architecture.

and maximize the dynamic range of the system. An analog dc offset cancelation circuit is proposed to solve this problem, and it will be discussed in detail in Section III-B.

B. Proposed Analog DC Offset Cancelation Circuit

Because the mixer output is single ended, the proposed analog dc offset cancelation circuit is designed to process single-ended input signal. A differential version of the analog dc offset cancelation circuit has been proposed in [28]. However, a single-ended design is preferred for interfacing with the radar RF front-end, which has single-ended baseband outputs. Fig. 3 shows the circuit diagram of the proposed single-ended circuit in this paper. The input signal V_{in} is connected to the level shifter output mentioned in Section II. $R1$ and $C1$ form an LPF to remove undesired high-frequency components from the mixer output. Following the LPF is a unit-gain buffer built with an op-amp OP1. This buffer can prevent any loading effect that may affect the performance of the preceding circuit and provides enough driving capability to drive the next stage. Another *RC* LPF formed by a resistor $R3$ and a capacitor $C3$ is used to extract dc information from the output of OP1. The cutoff frequency of this LPF should be smaller than the lowest signal frequency of interest. In case of vital signs sensing, the frequency of interest could be as low as 0.1 Hz. Therefore, $R3$ is chosen to be 2 MΩ and $C3$ is chosen to be 10 μF. This gives a cutoff frequency about 0.008 Hz. Since the time constant of an *RC* filter is inversely proportional to its cutoff

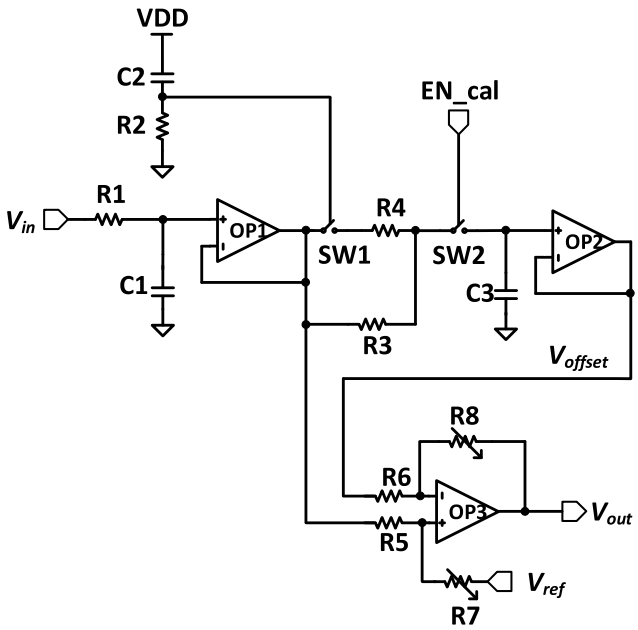

Fig. 3. Proposed dc-offset cancelation circuit.

frequency, a problem for using such a low cutoff frequency is that it takes a long time for the system to settle. The time constant is calculated to be 20 s for this LPF, and it will take 1 min for the system to settle within 5% of the final value after

being powered up. The settling time decides how much delay the biomedical radar sensor will need to function properly after it is enabled. For applications that require frequently power cycle the device, the settling time becomes a very important parameter.

To solve the slow settling problem, a fast-charging circuit is proposed to quickly charge the LPF holding capacitor $C3$ during power up. The fast-charging circuit consists of an RC high-pass filter (HPF) which senses the supply jump and a MOSFET switch SW1 that controls the fast-charging path. The HPF is formed by capacitor $C2$ and resistor $R2$. When the system is powered off, the supply is 0 V and the voltage on capacitor $C2$ is also 0 V. This is guaranteed by the design of the power on sequence and the supply switch. The mode control module will be enabled first, then the transceiver will be enabled, and the baseband circuit will be enabled at last. When the baseband circuit is disabled, the supply switch is connected to ground, whereas when it is enabled, the supply switch is connected to VDD. As soon as the baseband circuit is enabled, the HPF senses the supply jump from 0 V to VDD. Since the voltage on the capacitor $C2$ cannot jump abruptly, the HPF output must jump to VDD immediately. Therefore, the switch SW1 is turned on to let the buffer charge the holding capacitor $C3$ directly. After that, capacitor $C2$ will be slowly charged up through the resistor $R2$. After some time, the voltage on capacitor $C2$ will increase to VDD, and the switch SW1 is turned off automatically. The time constant of this HPF decides how long the fast-charge path will be on, which can be much smaller than the time constant of $C3$ and $R3$. But the time constant still needs to be long enough to allow adequate time for charging $C3$. Besides, $C2$ needs to be much larger than the parasitic capacitors on this node to ignore the capacitive-divider effect. In this design, $C2$ and $R2$ values are 1 μF and 200 KΩ, respectively.

However, shorting holding capacitor $C3$ to the buffer directly introduces another problem. Because the capacitance of $C3$ is very large, the output pole of the op-amp is pushed to lower frequency. It will cause stability issue for most op-amps. If the buffer starts ringing or oscillating, the final voltage on capacitor $C3$ will be unknown depending on when the switch is turned off. There are op-amps that can handle large capacitance, but usually they are more expensive. To reduce the design cost, a relatively small resistor $R4$ is added in series with switch SW1. When the fast-charging path is on, $R4$ and $C3$ introduce an additional zero. By properly choosing the value of $R4$, the impact of this pole and zero on the stability of the op-amp can be minimized. The larger the resistance of $R4$ is the better stability the op-amp will have. If $R4$ is infinite, then $C3$ is isolated from the op-amp completely. However, larger $R4$ also results in larger time constant from $R4$ and $C3$ and it leads to longer time to charge $C3$. So, there is a tradeoff between start-up time and stability. To minimize the charging time, the resistance of $R4$ needs to be as small as possible, under the condition that the stability of the buffer is good enough to avoid ringing. The final $R4$ value is chosen to be 1 KΩ in this design by simulating with the op-amps spice model. Hence, the time constant for $R4$ and $C3$ is 10 ms.

Ideally, after the fast-charging switch is turned off, the voltage on the capacitor $C3$ should be equal to the dc voltage of the input signal. However, there will be a small error depending on the ac component of the input signal and the time that the switch is turned off. After the fast-charging switch is turned off, $R3$ kicks in and the LPF formed by $C3$ and $R3$ starts to filter out the ac signal. In the end, the small error will gradually disappear if the cutoff frequency is low enough to filter out the ac signal completely.

To achieve a low cutoff frequency of the LPF formed by $C3$ and $R3$, the resistance of $R3$ needs to be large. This means that the LPF cannot provide enough driving capability. To overcome this problem, the output of this LPF is connected to another unit gain buffer built with op-amp OP2. Since the input source impedance is high for this op-amp, a low input bias current op-amp should be used here. In this design, a FET input op-amp with 2 pA maximum input bias current at room temperature is used, so that the voltage error is less than 4 μV. The output of OP2 is named as V_{offset}, which is equal to the dc value of the input signal

$$V_{\text{offset}} = V_{\text{in\_dc}}. \tag{7}$$

The last stage of the proposed baseband circuit is a difference amplifier as well as a VGA, which is built with another op-amp OP3. It subtracts V_{offset} from the input signal first, and then amplifies the difference signal. The gain is decided by the ratio of feedback resistor and input resistor of the difference amplifier. If $R5 = R6 = R_{\text{in}}$ and $R7 = R8 = R_{fb}$, then

$$V_{\text{out}} = \frac{R_{fb}}{R_{\text{in}}} \cdot (V_{\text{in}} - V_{\text{offset}}) + V_{\text{ref}} \tag{8}$$

where V_{ref} sets the common mode of this amplifier and it is chosen to be half of the supply voltage to allow the maximum swing for both the positive and the negative sides. The gain of this difference amplifier is adjustable by changing the resistance of R_{fb}. Based on the equation, the real input of the VGA is exactly the input signal minus its dc offset. Therefore, with the cancelation circuit, the VGA only sees an input without dc offset.

The proposed circuit tracks and removes the input dc offset automatically and continuously. As a result, even if the signals of interest have useful slow variation dc components, it will still be removed from the final output V_{out} as it cannot be distinguished from the undesired dc offset. Equivalently, it emulates a high-pass signal transfer function. This is the same as running the adaptive feedback loop continuously. Since the entire system is dc-coupled, the circuit can be easily reconfigured to pass through the input signal dc change. In applications that require precise information including dc and low-frequency components, the LPF can be connected or disconnected in a controlled manner through switch SW2. After the baseband is enabled and settled, the cancelation circuit can be disabled by opening switch SW2. The holding capacitor $C3$ can hold the voltage if leakage current is negligible. By doing this, the initial dc offset will be removed, whereas the future slow change in signal dc can pass through. This is the same as enabling the adaptive feedback loop first to find out the correct hardware setting without

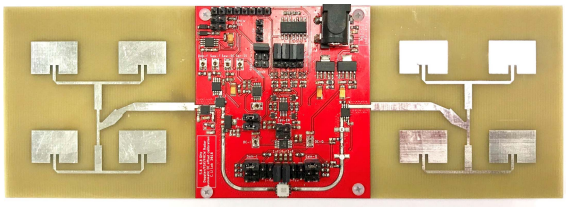

Fig. 4. Prototype of the proposed biomedical radar sensor.

saturation, then disabling the adaptive feedback loop to record dc input information.

IV. Experiment Setup and Measurement Results

To demonstrate the performance of the proposed biomedical radar sensor and analog dc offset cancelation circuit, several experiments were carried out with a fabricated integrated prototype, which uses a 5-V power supply. Hence the ideal common mode of the prototype is 2.5 V. A photograph of the prototype is shown in Fig. 4. All the output signals from the biomedical radar sensor were sampled through an NI USB-6009 acquisition unit. Then postprocessing and signal display were performed in MALAB.

A. DC Offset Cancelation

The dc offsets presented at the I/Q channel outputs of the mixer were measured by placing a corner reflector at various ranges from 0.5 to 2 m in front of the radar. The minimum and maximum dc offsets were found to be -0.6 and 0.6 V, respectively, for both channels, which included both hardware imperfection and clutter reflections. After passing the level shifters, the signals from the mixer were shifted up to positive operation range centered at the middle of the supply voltages, which was 2.5 V. Since the outputs of the level shifters are connected to the input Vin of the proposed dc offset cancelation circuit shown in Fig. 3, the dc offset range expected in Vin is estimated to be from 1.9 to 3.1 V. The theoretical dc offset can be larger depending on the components' operational ranges.

In the first experiment, the transceiver of the biomedical radar sensor prototype was bypassed, and the test only focused on the analog dc offset cancelation circuit. A dc voltage sweep was performed to characterize the dc performance of the proposed analog dc offset cancelation circuit. A dc voltage source was connected to input V_{in} of Fig. 3 and the voltage was slowly swept from 0.5 to 4.5 V. The output V_{out} was measured by a dc meter. The dc transfer function between the input and output is plotted in Fig. 5, the x-axis is the input voltage and the y-axis is the corresponding output voltage. As can be seen, with a wide range of input dc offset (i.e., from 1 to 4 V), the output dc voltage is stably kept at 2.5 V. Only at the extreme of input sweep range (i.e., below 1 V or beyond 4 V), the dc transfer function starts to bend and exhibits some error at the output. The reason for the output error with extreme input voltage is that the op-amps start to see headroom issue when its output tries to establish a voltage close to the supply rails. This can be improved by increasing the supply voltage or choosing rail-to-rail op-amps.

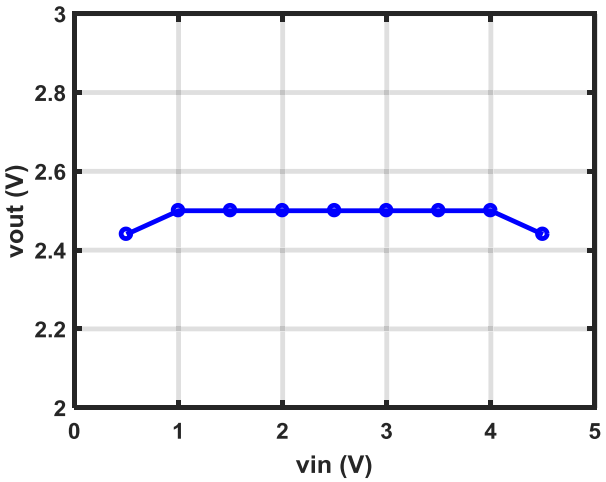

Fig. 5. Measured dc transfer function of the proposed dc offset cancelation circuit.

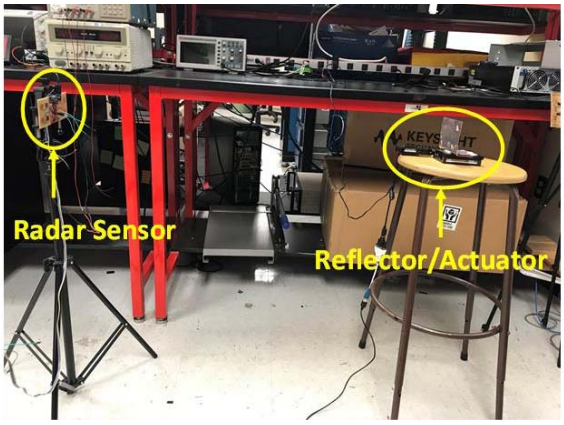

Fig. 6. Experiment setup with an actuator controlling a reflector.

This experiment verified that the proposed analog dc offset cancelation circuit can effectively remove the dc offset over a wide input range.

B. Radar Sensor Dynamic Range Improvement

This experiment was performed with the entire biomedical radar sensor. An actuator controlling a reflector was used as the target to generate precisely controlled movement amplitude and frequency. The experiment setup is shown in Fig. 6. The biomedical radar sensor was configured in the Doppler mode and placed to face the reflector at 0.5 m distance. In this experiment, the transmit frequency of the VCO was 5.8 GHz and the reflector moved in horizontal direction with a 0.9 Hz frequency and a 0.5 mm movement amplitude. The output of mixer was around 0.3 V. The VGA gain was set as 20 dB. Those parameters were chosen so that the VGA output was close to its maximal swing. Instead of trying to add different dc offset to the system, which is difficult to control, V_{offset} in Fig. 3 was shifted up and down by forcing the ungrounded terminal of $C3$ with a voltage source. The outputs of the VGA were recorded under different conditions. With analog dc offset cancelation disabled, if V_{offset} is skewed to be higher

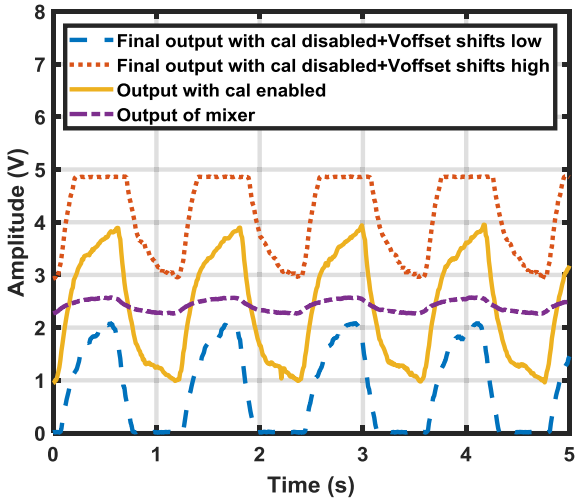

Fig. 7. Experiment demonstrating dynamic range improvement with a skewed common mode voltage.

than the common mode of the mixer output, the baseband output will saturate in the lower half cycle; if V_{offset} is skewed to be lower than the common mode of the mixer output, the baseband output will saturate in the upper half cycle. With analog dc offset cancelation enabled, as long as V_{offset} is within the working range found in the first experiment, the baseband output is always recentered at the middle of the supply rails. The results are shown in Fig. 7. This demonstrated that the dc offset in the proposed biomedical radar sensor can be removed automatically and the dynamic range of the system can be maximized.

C. Fast-Settling Measurement

Settling behavior with and without the fast-charging technique is compared in this experiment. The experiment started with the baseband circuit in the power-off state with a dc offset applied to V_{in} in Fig. 3. Then, the baseband circuit was enabled to observe the baseband circuit output V_{out} in Fig. 3. The fast-charging circuit will be automatically triggered after the system is enabled. To emulate a conventional design without fast charging, the output of the HPF formed by $R2$ and $C2$ in Fig. 3 was forced to 0 V by an external voltage source. Fig. 8(a) shows the settling behavior without fast charging. Fig. 8(b) shows the setting behavior with the fast charging and the output of the HPF which controls the fast-charging path. The result clearly shows that the fast-charging circuit can significantly reduce the settling time of the system. As can be seen, without fast-charging feature, the output settling time constant is about 20 s; with fast-charging feature, the HPF time constant is about 0.2 s, while the output settling time constant is about 10 ms.

D. Vital Signs Detection

To further demonstrate the effectiveness of the proposed biomedical radar, a remote human's vital signs monitoring experiment was conducted in a typical lab environment. In this experiment, a human subject was seated around 1 m in front

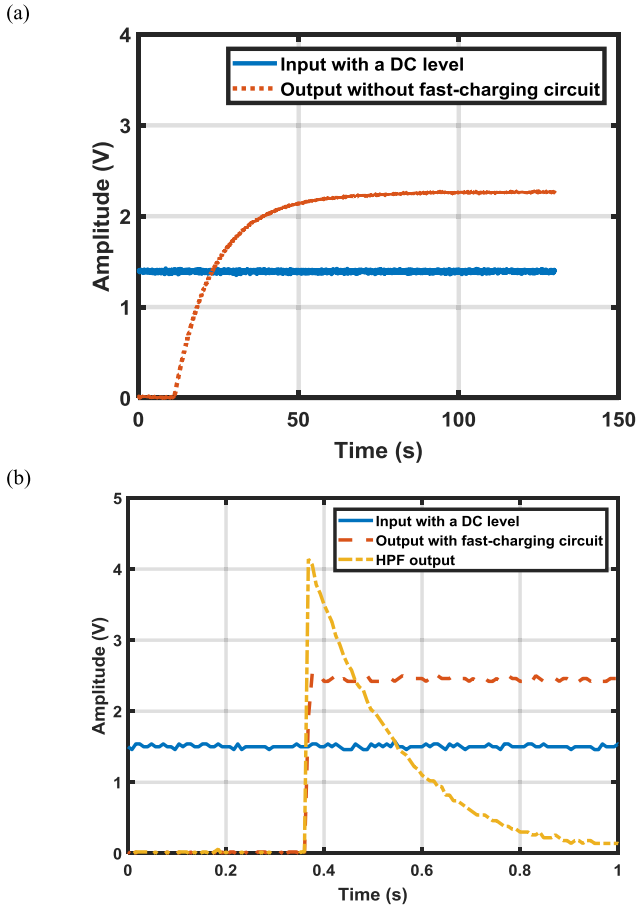

Fig. 8. (a) Output settling without fast charging. (b) Output settling with fast-charging circuit enabled.

of the radar. A photograph of the experiment setup is shown in Fig. 9(a). Both the I and Q outputs of the biomedical sensor were recorded and presented in Fig. 9(b). The system was powered on around 16 s. It should be noted that for a conventional ac-coupled Doppler biomedical radar, the settling time could be as long as power on period, which means no valuable data could be acquired for a conventional design in this scenario. In contrast, shortly after the proposed radar was powered on (i.e., within 100 ms), the outputs common mode directly jumped to the middle voltage of supply rails with the help of the fast charging circuit in this design. Because of the analog dc offset cancelation circuit, the output common mode was always fixed at the optimal value independent of clutter reflection and the distance between the human subject and the biomedical sensor. Hence the dynamic range of the biomedical radar can always be maximized. The dc offset cancelation was carried out automatically after powering-up without extra configuration. In Fig. 9(b), the Q channel output was close to its maximal possible swing. It should be noted that, due to the residue phase in Doppler detection [14], it is normal for the I/Q channels to have different signal amplitude. As a matter of fact, one of the channels could have nearly no signal at certain detection distance. This is the reason for using quadrature channel demodulation for Doppler biomedical radar [14].

Fast Fourier transform (FFT) was applied to the complex signal combined from the I/Q channels. Respiration rate

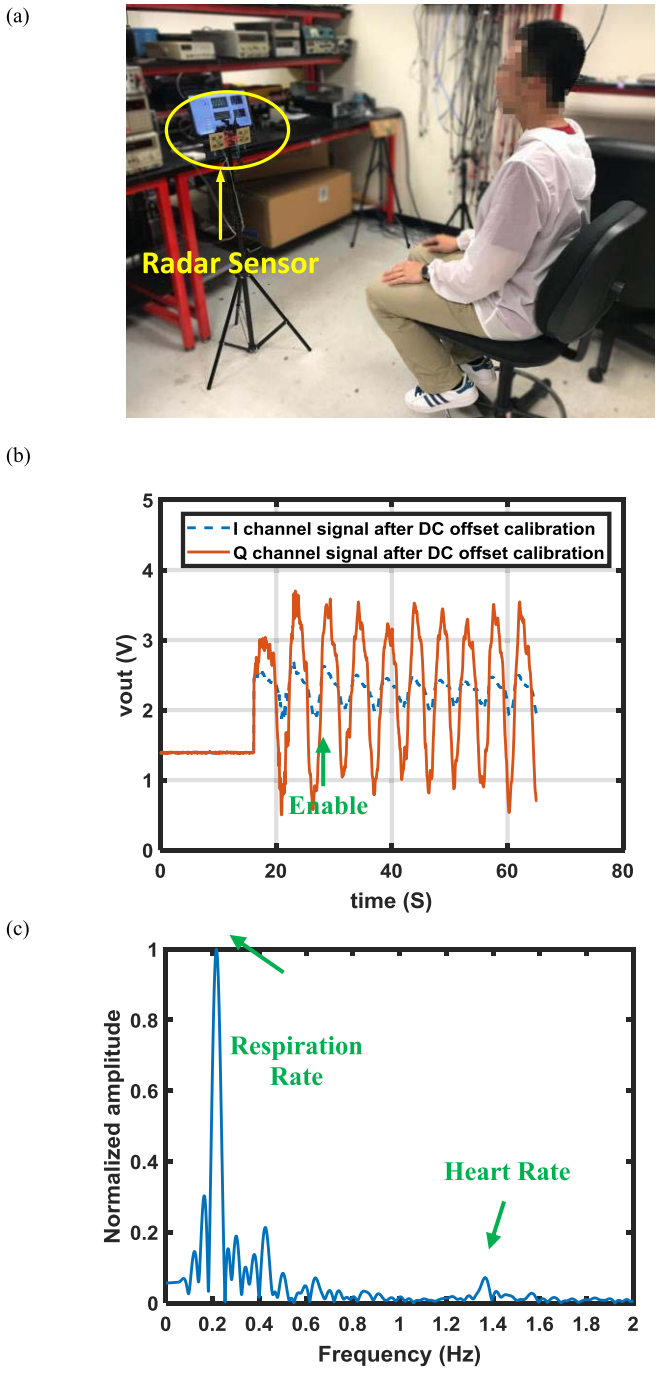

Fig. 9. (a) Experiment setup of vital signs sensing. (b) Recorded I/Q channel transient waveform for vital signs sensing with the proposed biomedical radar sensor. (c) Spectrum of the sensor output data.

of around 0.22 Hz and heart rate of about 1.36 Hz can be clearly identified in the FFT frequency spectrum in Fig. 9(c), which corresponds to 13 breaths and 81 heart beats per minutes, respectively. The same experiment was repeated for five different human subjects wearing a heart rate fingertip sensor as a reference. The results are shown in Fig. 10.

E. DC Input Sensing

To demonstrate the proposed biomedical radar's capability to precisely record dc input, a dc input needs to be generated.

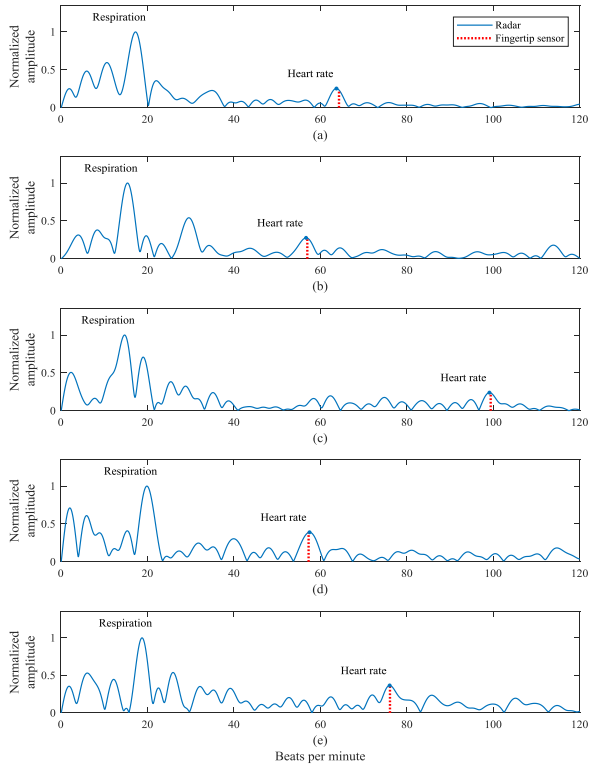

Fig. 10. Spectra of the radar sensor output for five different human subjects and their corresponding reading from heart rate fingertip sensor.

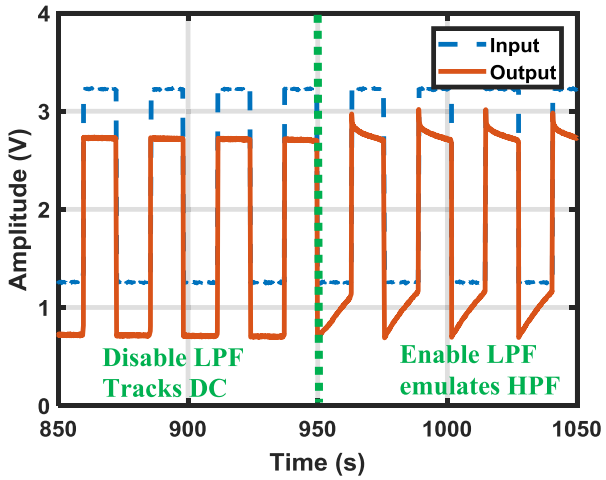

Fig. 11. DC tracking using the proposed biomedical radar sensor.

However, since it is difficult to generate a clean step function from a real target, a square wave generator was used in this experiment. The input of the baseband circuit was connected to the square wave generator, and it can be accurately controlled to avoid uncertainty. The frequency of the square wave was set low so that the voltage level is fixed for a relatively long time. As discussed in Section III, the analog dc offset cancelation does not distinguish whether a dc voltage is from the input signal or the circuit itself, so the dc input will also be removed. To sense the input dc offset, the LPF needs to be disabled. The experiment was carried out with a 0.04 Hz square wave input. After the system is turned on, the LPF was disabled first, then enabled. The result is plotted in Fig. 11. As can

be seen, the first half of the waveform was generated when the LPF was disabled. The output signal was able to track the input dc change without any distortion. The level shift between the input and the output signals is because of the dc offset in the system. This voltage shift is desirable so that the output achieves the maximum dynamic range. The second half of the waveform was generated when the LPF was enabled. When the dc input changed, the analog cancelation circuit was trying to remove it. The output is distorted in this case.

V. Conclusion

In this paper, a high dynamic range biomedical radar sensor with analog dc offset cancelation circuit is proposed to eliminate the dc offsets in a dc-coupled homodyne receiver. A board-level integrated prototype was fabricated and tested. The experiment results demonstrated that the proposed sensor can automatically correct a wide range of dc offset and achieve an improved dynamic range with a short settling time. Vital signs sensing was also presented with a human subject to show the robustness of the proposed architecture. On the other hand, the ability to record input dc change without distortion was verified with a slow square wave input. One area of future work will focus on exploring other advantages of dc-coupled biomedical radar sensor with analog dc offset cancelation, such as in the FMCW mode and the FSK mode. Moreover, the analog dc offset cancelation scheme can be expanded to nonradar circuits that face similar challenges due to dc offsets.

References

[1] J. C. Lin, "Noninvasive microwave measurement of respiration," *Proc. IEEE*, vol. 63, no. 10, p. 1530, Oct. 1975.

[2] H.-R. Chuang, Y. F. Chen, and K.-M. Chen, "Automatic clutter-canceler for microwave life-detection systems," *IEEE Trans. Instrum. Meas.*, vol. 40, no. 4, pp. 747–750, Aug. 1991.

[3] J. C. Lin, "Microwave sensing of physiological movement and volume change: A review," *Bioelectromagnetics*, vol. 13, no. 6, pp. 557–565, 1992.

[4] C. Li, V. M. Lubecke, O. Boric-Lubecke, and J. Lin, "A review on recent advances in Doppler radar sensors for noncontact healthcare monitoring," *IEEE Trans. Microw. Theory Techn.*, vol. 61, no. 5, pp. 2046–2060, May 2013.

[5] Z. Peng *et al.*, "A portable FMCW interferometry radar with programmable low-IF architecture for localization, ISAR imaging, and vital sign tracking," *IEEE Trans. Microw. Theory Techn.*, vol. 65, no. 4, pp. 1334–1344, Apr. 2017.

[6] Z. Peng, L. Ran, and C. Li, "A *K*-band portable FMCW radar with beamforming array for short-range localization and vital-Doppler targets discrimination," *IEEE Trans. Microw. Theory Techn.*, vol. 65, no. 9, pp. 3443–3452, Sep. 2017.

[7] T. Mitomo, N. Ono, H. Hoshino, Y. Yoshihara, O. Watanabe, and I. Seto, "A 77 GHz 90 nm CMOS transceiver for FMCW radar applications," *IEEE J. Solid-State Circuits*, vol. 45, no. 4, pp. 928–937, Apr. 2010.

[8] Y. Wang, Q. Liu, and A. E. Fathy, "CW and pulse–Doppler radar processing based on FPGA for human sensing applications," *IEEE Geosci. Remote Sens.*, vol. 51, no. 5, pp. 3097–3107, May 2013.

[9] J. Wang, Y. Tang, J.-M. Muñoz-Ferreras, R. Gómez-García, and C. Li, "An improved indoor localization solution using a hybrid UWB-Doppler system with Kalman filter," in *Proc. IEEE Radio Wireless Symp. (RWS)*, Anaheim, CA, USA, Jan. 2018, pp. 181–183.

[10] J. Wang and C. Li, "A human tracking and physiological monitoring FSK technology for single senior at home care," in *Proc. 40th Annu. Int. Conf. IEEE Eng. Med. Biol. Soc.*, Jul. 2018, pp. 4432–4435.

[11] G. Vinci *et al.*, "Six-port radar sensor for remote respiration rate and heartbeat vital-sign monitoring," *IEEE Trans. Microw. Theory Techn.*, vol. 61, no. 5, pp. 2093–2100, May 2013.

[12] F. Barbon, G. Vinci, S. Lindner, R. Weigel, and A. Koelpin, "A six-port interferometer based micrometer-accuracy displacement and vibration measurement radar," in *IEEE MTT-S Int. Microw. Symp. Dig.*, Montreal, QC, Canada, Jun. 2012, pp. 1–3.

[13] M.-C. Tang, F.-K. Wang, and T.-S. Horng, "Single self-injection-locked radar with two antennas for monitoring vital signs with large body movement cancellation," *IEEE Trans. Microw. Theory Techn.*, vol. 65, no. 12, pp. 5324–5333, Dec. 2017.

[14] M.-C. Tang, C.-Y. Kuo, D.-C. Wun, F.-K. Wang, and T.-S. Horng, "A self- and mutually injection-locked radar system for monitoring vital signs in real time with random body movement cancellation," *IEEE Trans. Microw. Theory Techn.*, vol. 64, no. 12, pp. 4812–4822, Dec. 2016.

[15] M. Mercuri *et al.*, "A direct phase-tracking Doppler radar using wavelet independent component analysis for non-contact respiratory and heart rate monitoring," *IEEE Trans. Biomed. Circuits Syst.*, vol. 12, no. 3, pp. 632–643, Jun. 2018.

[16] P. J. Soh, G. A. E. Vandenbosch, M. Mercuri, and D. M. M.-P. Schreurs, "Wearable wireless health monitoring: Current developments, challenges, and future trends," *IEEE Microw. Mag.*, vol. 16, no. 4, pp. 55–70, May 2015.

[17] M. Mercuri, Y.-H. Liu, I. Lorato, T. Torfs, A. Bourdoux, and C. van Hoof, "Frequency-tracking CW Doppler radar solving small-angle approximation and null point issues in non-contact vital signs monitoring," *IEEE Trans. Biomed. Circuits Syst.*, vol. 11, no. 3, pp. 671–680, Jun. 2017.

[18] A. Rahman, V. Lubecke, E. Yavari, X. Gao, and O. Boric-Lubecke, "High dynamic range DC coupled CW Doppler radar for accurate respiration characterization and identification," in *Proc. 89th ARFTG Microw. Meas. Conf. (ARFTG)*, Honolulu, HI, USA, Jun. 2017, pp. 1–4.

[19] Y. Yang, C. Gu, Y. Li, R. Gale, and C. Li, "Doppler radar motion sensor with CMOS digital DC-tuning VGA and inverter-based sigma-delta modulator," *IEEE Trans. Instrum. Meas.*, vol. 63, no. 11, pp. 2666–2674, Nov. 2014.

[20] A. D. Droitcour, O. Boric-Lubecke, V. M. Lubecke, J. Lin, and G. T. A. Kovacs, "Range correlation and I/Q performance benefits in single-chip silicon Doppler radars for noncontact cardiopulmonary monitoring," *IEEE Trans. Microw. Theory Techn.*, vol. 52, no. 3, pp. 838–848, Mar. 2004.

[21] H.-C. Kuo *et al.*, "A fully integrated 60-GHz CMOS direct-conversion Doppler radar RF sensor with clutter canceller for single-antenna noncontact human vital-signs detection," *IEEE Trans. Microw. Theory Techn.*, vol. 64, no. 4, pp. 1018–1028, Apr. 2016.

[22] C. Li, Y. Xiao, and J. Lin, "A 5GHz double-sideband radar sensor chip in 0.18 μm CMOS for non-contact vital sign detection," *IEEE Microw. Wireless Compon. Lett.*, vol. 18, no. 7, pp. 494–496, Jul. 2008.

[23] C. Li, X. Yu, C.-M. Lee, D. Li, L. Ran, and J. Lin, "High-sensitivity software-configurable 5.8-GHz radar sensor receiver chip in 0.13-μm CMOS for noncontact vital sign detection," *IEEE Trans. Microw. Theory Techn.*, vol. 58, no. 5, pp. 1410–1419, May 2010.

[24] T.-Y. J. Kao, Y. Yan, T.-M. Shen, A. Y.-K. Chen, and J. Lin, "Design and analysis of a 60-GHz CMOS Doppler micro-radar system-in-package for vital-sign and vibration detection," *IEEE Trans. Microw. Theory Techn.*, vol. 61, no. 4, pp. 1649–1659, Apr. 2013.

[25] B.-K. Park, O. Boric-Lubecke, and V. M. Lubecke, "Arctangent demodulation with DC offset compensation in quadrature Doppler radar receiver systems," *IEEE Trans. Microw. Theory Techn.*, vol. 55, no. 5, pp. 1073–1079, May 2007.

[26] C. Gu, R. Li, S. B. Jiang, and C. Li, "A multi-radar wireless system for respiratory gating and accurate tumor tracking in lung cancer radiotherapy," in *Proc. Annu. Int. Conf. IEEE Eng. Med. Biol. Soc.*, Boston, MA, USA, Aug./Sep. 2011, pp. 417–420.

[27] Z.-P. Yang and Y.-C. Chiang, "Vital signal radar with adaptive compensation circuits to effectively eliminate DC offsets," *IEEE Microw. Wireless Compon. Lett.*, vol. 28, no. 1, pp. 88–90, Jan. 2018.

[28] D. Tang, J. Wang, Z. Peng, Y.-C. Chiang, and C. Li, "A DC-coupled biomedical radar sensor with analog DC offset calibration circuit," in *Proc. IEEE Int. Instrum. Meas. Technol. Conf. (I2MTC)*, Houston, TX, USA, May 2018, pp. 1–6.

[29] P.-H. Wu, J.-K. Jau, C.-J. Li, T.-S. Horng, and P. Hsu, "Phase- and self-injection-locked radar for detecting vital signs with efficient elimination of DC offsets and null points," *IEEE Trans. Microw. Theory Techn.*, vol. 61, no. 1, pp. 685–695, Jan. 2013.

[30] C. Gu *et al.*, "Accurate respiration measurement using DC-coupled continuous-wave radar sensor for motion-adaptive cancer radiotherapy," *IEEE Trans. Biomed. Eng.*, vol. 59, no. 11, pp. 3117–3123, Nov. 2012.
[31] C. C. Enz and G. C. Temes, "Circuit techniques for reducing the effects of op-amp imperfections: Autozeroing, correlated double sampling, and chopper stabilization," *Proc. IEEE*, vol. 84, no. 11, pp. 1584–1614, Nov. 1996.
[32] M. C. Budge and M. P. Burt, "Range correlation effects on phase and amplitude noise," in *Proc. Southeastcon*, Charlotte, NC, USA, 1993, p. 5
[33] W. Xu, C. Gu, C. Li, and M. Sarrafzadeh, "Robust Doppler radar demodulation via compressed sensing," *Electron. Lett.*, vol. 48, no. 22, pp. 1428–1430, Oct. 2012.
[34] J. Wang, X. Wang, L. Chen, J. Huangfu, C. Li, and L. Ran, "Noncontact distance and amplitude-independent vibration measurement based on an extended DACM algorithm," *IEEE Trans. Instrum. Meas.*, vol. 63, no. 1, pp. 145–153, Jan. 2014.
[35] H.-C. Chen, T. Wang, and S.-S. Lu, "A 5–6 GHz 1-V CMOS direct-conversion receiver with an integrated quadrature coupler," *IEEE J. Solid-State Circuits*, vol. 42, no. 9, pp. 1963–1975, Sep. 2007.

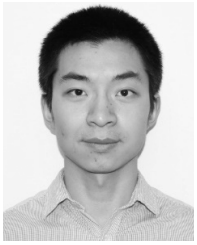

Dongyang Tang (S'18) received the B.Sc. degree in microelectronics from Sichuan University, Chengdu, China, in 2011, the M.Sc. degree in electrical engineering from the University of Michigan, Ann Arbor, MI, USA, in 2013. He is currently pursuing the Ph.D. degree in electrical engineering from Texas Tech University, Lubbock, TX, USA.

His current research interest includes mixed-signal integrated circuit, RF circuits, and radar systems.

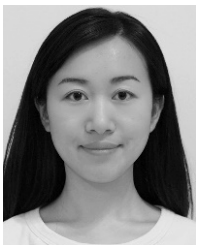

Jing Wang (S'17) received the B.S. degree in communication engineering from the Fujian University of Technology, Fuzhou, China, in 2015. She is currently pursuing the Ph.D. degree in electrical engineering with Texas Tech University, Lubbock, TX, USA.

Her current research interests include microwave circuits, wireless RF sensors, and their biomedical applications.

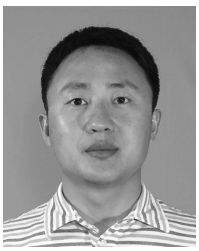

Weibo Hu (S'12–M'14) received the bachelor's degree from the Harbin Institute of Technology, Harbin, China, in 2005, and the master's degree from Peking University, Beijing, China, in 2008, respectively, the Ph.D. from Texas Tech University, Lubbock, TX, USA, in 2014.

He was with the Mixed-Signal Department, Qualcomm, San Diego, CA, USA, He was a Faculty Member, Nankai University, Tianjin, China, in 2017, where he is currently a Professor with the Microelectronics Department and a Director of integrated circuits and systems. His current research interests include mixed-signal integrated circuit and system design. Besides designing different mixed-signal blocks, his lab tries to develop circuits or systems to mimic human thinking and sensing, such as implementing artificial intelligence chips and small radar-based sensing systems.

Zhengyu Peng (S'15) received the B.S. and M.Sc. degrees in electrical engineering from Zhejiang University, Hangzhou, China, in 2011 and 2014, respectively, and the Ph.D. degree in electrical engineering from Texas Tech University, Lubbock, TX, USA, in 2018.

He is currently a Senior Radar System Engineer with Aptiv Corporation, Kokomo, IN, USA. His current research interests include portable radar systems, antennas, microwave circuits, and biomedical applications of microwave/RF circuits and systems.

Dr. Peng was a recipient of the 2016 IEEE Microwave Theory and Techniques Society Graduate Fellowship, the third place of the Student Design Competition for high sensitivity radar in 2015 IEEE International Microwave Symposium, and the Excellent Demo Track Presentation Award in 2016 IEEE Radio and Wireless Week. He is a Reviewer for several IEEE publications, including the IEEE Transactions on Microwave Theory and Techniques, the IEEE Transactions on Instrumentation and Measurement, the IEEE Transactions on Circuits and Systems II, the IEEE Antennas and Wireless Propagation Letters, the IEEE Microwave and Wireless Components Letters, the IEEE Sensors Journal, the IEEE Journal of Electromagnetics, RF, and Microwaves in Medicine and Biology, and the IEEE Journal on Emerging and Selected Topics in Circuits and Systems

Yi-Chyun Chiang (M'87–SM'14) received the B.S. degree in marine technology and the M.S. and Ph.D. degrees in electronic engineering from National Chiao-Tung University, Hsin-Chu, Taiwan, in 1982 and 1992, respectively,

He is currently a Professor with the Department of Electronic Engineering, Chang Gung University, Tao-Yuan, Taiwan. His current research interests include the development of design methods in realization of high-performance microwave passive and active components; as well as the new type of noncontact vital signal detection systems.

Dr. Chiang is listed in 2006 and 2017 Marquis Who's who in World and IBC Top 100 Engineers in 2008.

Changzhi Li (S'06–M'09–SM'13) received the B.S. degree in electrical engineering from Zhejiang University, Hangzhou, China, in 2004, and the Ph.D. degree in electrical engineering from the University of Florida, Gainesville, FL, USA, in 2009.

From 2007 to 2009, he was with Alereon Inc., Ausitn, TX, USA, and with Coherent Logix Inc., Austin, TX, USA, where he was involved in ultra-wideband transceivers and software-defined radio. In 2009, He joined Texas Tech University, Lubbock, TX, USA, as an Assistant Professor, where he became an Associate Professor in 2014. His current research interests include the biomedical applications of microwave technology, wireless sensors, and RF/analog circuits.

Dr. Li was a recipient of the IEEE Microwave Theory and Techniques Society (MTT-S) Outstanding Young Engineer Award, the IEEE Sensors Council Early Career Technical Achievement Award, the ASEE Frederick Emmons Terman Award, the IEEE-HKN Outstanding Young Professional Award, the NSF Faculty Early CAREER Award, and the IEEE MTT-S Graduate Fellowship Award. He is an Associate Editor of the IEEE TRANSACTIONS ON MICROWAVE THEORY AND TECHNIQUES, the IEEE TRANSACTIONS ON CIRCUITS AND SYSTEMS I, and the IEEE JOURNAL OF ELECTROMAGNETICS, RF AND MICROWAVES IN MEDICINE AND BIOLOGY. He served as an Associate Editor of the IEEE TRANSACTIONS ON CIRCUITS AND SYSTEMS II from 2014 to 2015. He served as a TPC Co-Chair for the IEEE MTT-S International Microwave Biomedical Conference in 2018 and the IEEE Wireless and Microwave Technology Conference from 2012 to 2013.